ORIGINAL ARTICLE

Journal Section

# Deciphering SH-SY5Y neuroblastoma cell proliferation: A detailed investigation of seeding concentrations, cultivation surfaces, and long-term maintenance in a sealed chamber

**Ewelina Kalwarczyk[1*] | Agnieszka Lukasiak[1] | Damian Woznica[1] | Weronika Switlik[2] | Julia Anchimowicz[2] | Piotr Zielonka[1] | Slawomir Jakiela[1*]**

[1]Department of Physics and Biophysics, Institute of Biology, Warsaw University of Life Sciences, 159 Nowoursynowska Street, 02776 Warsaw, Poland

[2]Department of Biochemistry and Microbiology, Institute of Biology, Warsaw University of Life Sciences, 159 Nowoursynowska Street, 02776 Warsaw, Poland

**Correspondence**
Elwelina Kalwarczyk and Slawomir Jakiela, Department of Physics and Biophysics, Institute of Biology, Warsaw University of Life Sciences, 159 Nowoursynowska Street, 02776 Warsaw, Poland
Email: ewelina_kalwarczyk@sggw.edu.pl; slawomir_jakiela@sggw.edu.pl

**Funding information**
National Science Centre, Poland, SONATA BIS 9, Grant/Award Number: 2019/34/E/ST4/00281

This study investigated the proliferation dynamics of SH-SY5Y neuroblastoma cells in a confined environment. The effects of seeding concentrations, culture surfaces and long-term maintenance in a sealed chamber were systematically investigated. Seeding concentration experiments revealed a clear correlation between initial cell number and proliferation rate, highlighting the importance of precise adjustments for optimal cell culture results. The study of available surface effects showed a nuanced relationship between chamber dimensions and cell growth, with confluence stability observed in larger chambers with diameters greater than 10 mm. The study also compared SH-SY5Y cells with HeLaGFP and 16HBE14$\sigma$ cells, revealing growth patterns influenced by chamber size. A properly designed sealed chamber with continuous real-time microscopic monitoring showed comparable cell growth to standard culture chambers. The research provides valuable insights into optimising SH-SY5Y cell culture practices, particularly in microfluidic systems.

# 1 | INTRODUCTION

In cell biology and bioengineering, traditional microscopic studies using fixed biological preparations have long been the gold standard for assessing the impact of compounds on cell function and viability [1]. However, this approach inherently limits the ability to observe dynamic processes occurring in real time. Enter microfluidic technology, which seamlessly integrates microscopic observation with precise drug delivery [2;3]. This breakthrough makes it possible to continuously monitor the influence of different toxins or drugs on cell function [4]. Taking this a step further, organ-on-a-chip systems mimic tissue systems and provide insights into their response to induced disease [5;6].

The authors sought to use microfluidic techniques in their study of SH-SY5Y cells, chosen as a model for neurodegenerative diseases [7;8]. In basic research into neurodegenerative diseases, the choice of an appropriate model system is crucial [9;10]. Both human and animal cells are used, including primary and immortalised lines. The human immature neuroblastoma cell line SH-SY5Y, widely used in Parkinson's and Alzheimer's disease research [11;12], can be modified to mimic dopaminergic [13;14] or cholinergic [15;16] states, making it particularly valuable for studying toxic protein aggregation [17;18] and mitochondrial dysfunction [19;20]. However in our preliminary experiments, culturing SH-SY5Y cells in small microfluidic chambers (including polycarbonate, PDMS and glass substrates with and without surface modification) showed a significantly slower proliferation rate (over 10-fold) compared to standard dishes. As a result, a series of calibration studies were performed to determine the optimal chamber size to achieve cell proliferation comparable to that observed in conventional culture dishes.

Studies using SH-SY5Y cells in microfluidic systems have predominantly used polydimethylsiloxane (PDMS) [21;22] substrates or PDMS-glass combinations [23;24]. Alternative materials such as cycloolefin polymers [25] and Noland optical adhesive 81 (NOA 81) [26] have also been used. Surface treatments to enhance cell adhesion such as poly-L-lysine [27;28], fibronectin [21;29], polyornithine [27] or extracellular matrix coating [25] are commonly used. Notably, there is a paucity of research investigating SH-SY5Y cells in microfluidic systems without additional surface treatment.

The studies presented herein provide compelling insights into the proliferation of SH-SY5Y cells within meticulously crafted polycarbonate chambers of varying diameters (from 3mm to 50mm). Importantly, these chambers were used without any additional surface treatment to enhance cell adhesion. Comparative analysis of cell growth in these chambers versus conventional 60 mm diameter Petri dishes (Corning) was performed. All images capturing the coverage of the test media during successive days of culture are available in the Zenodo repository [30]. Real-time monitoring of cell growth was facilitated by a phase-contrast microscope, and growth kinetics were methodically analysed by comprehensive examination of microscopic images.

In addition, the respiration of SH-SY5Y cells was studied using the Oroboros Oxygraph-2k device. This study aimed to elucidate oxygen consumption in the culture medium by a population of cells in a sealed chamber, preventing gas exchange. Over an observation period of one week, the growth of SH-SY5Y cells was investigated in an airtight polycarbonate chamber specifically designed for targeted studies in microfluidic systems. In addition, a video showing the growth of SH-SY5Y cell cultures, with individual culture frames recorded every 5 minutes, has been deposited in the Zenodo repository [31].

The research carried out seems important in the fields of cell biology and bioengineering, particularly as we move the culture into small microfluidic systems. These systems offer remarkable opportunities for observing cellular responses to drugs in the diseases being studied [4]. However, they also present a significant challenge for cell function in confined spaces [32], a point highlighted in this article.

# 2 | MATERIALS AND METHODS

## 2.1 | Materials

The following chemicals and solutions were provided by Sigma-Aldrich, Germany: Dulbecco's modified Eagle's medium (DMEM) - D6546, Eagle's minimum essential medium (MEM) - M4655, heat inactivated fetal bovine serum (FBS) - F9665, L-glutamine solution, 200 mM - G7513, antibiotics solution containing 10 000 units of penicillin, 10 mg/mL streptomycin - P0781, MEM Non-

Essential Amino Acid (NEAA) - M7145, Trypsin-EDTA solution - T3924, sodium dodecyl sulphate (SDS) - L3771, dichloromethene – 650463, Oligomycin - O4876, carbonyl cyanide 4-(trifluoromethoxy)phenylhydrazone (FCCP) - R8875, and antimycin A - A8674. Ethyl alcohol, 96% was obtained from POCH, Poland (396420113), phosphate buffered saline (PBS) without calcium and magnesium was purchased from Lonza.

## 2.2 | Cells

Three cell lines were used in a controlled laboratory environment to study cellular responses. The initial cell line, SH-SY5Y human neuroblastoma, was obtained from ECACC and cultured in DMEM with 10% FBS, 1% 200 mM L-glutamine, 1% antibiotic solution and 1% NEAA for optimal growth and viability.

In addition, the study included the Milipore 16HBE14$\sigma$ human bronchial epithelial cell line, which was cultured in MEM with 10% FBS and 1% antibiotics solution to diversify cellular components and increase the breadth of the study.

A third cell line, HeLaGFP inducible GFP HeLa stable, purchased from GenTarget Inc., was cultured in DMEM with 10% FBS, 1% 200 mM L-glutamine and 1% antibiotics solution.

Cell growth was continuously monitored using an Olympus CKX53 phase-contrast microscope with a DLT camera (Delta Optical, DLT-Cam PRO 1080 HDMI USB) in a temperature-controlled chamber set at 37 °C as per experimental requirements.

## 2.3 | Chambers

In our investigation, cellular cultures were cultivated in diverse vessels, encompassing commercially available cell culture dishes, such as NUNC Easy Flasks (75 $cm^2$) and Nunc MicroWell 96-Well Microplates obtained from Thermo Scientific. Additionally, we employed 60 mm petri dishes from Corning. Taking a more tailored approach, our research incorporated the use of specially designed multi-chamber cultures (see Figure 1). These chambers were carefully crafted with precision by milling 10 mm and 5 mm thick polycarbonate plates (Makrolon, Bayer, Leverkusen, Germany) using a state-of-the-art CNC milling machine (MSG4025, Ergwind, Gdansk, Poland). To mitigate evaporation of the medium and emulate conditions akin to a standard Petri dish for cell culture, these chambers were fitted with a polycarbonate lid.

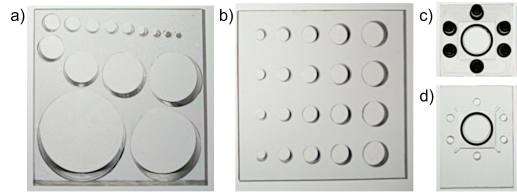


**FIGURE 1** Photographs depicting a custom-designed multi-chamber culture dish carefully crafted from polycarbonate using CNC milling are presented herein. The culture dish comprises the following components: a) A 15-well multi-chamber with varying chamber diameters ranging from 2.4 to 50 mm. The diameters include: 2.4, 3, 4, 5, 6, 7, 8, 9, 10, 15, 20, 25, 30, 40, and 50 mm. b) A 20-well chamber featuring diameters of 6, 8, 10, 12, and 15 mm. Notably, each diameter is replicated four times, facilitating comparative experiments. c) The top layer and d) the bottom layer of a hermetically sealed polycarbonate chamber with a diameter of 12 mm are also showcased. These chambers were sealed using an O-ring and secured together with 6 M3 screws.

# 3 | EXPERIMENTAL

## 3.1 | Fabrication of multi-chamber cell dish

In order to enhance the prepared culture dishes, their surfaces underwent a smoothing process facilitated by a methylene chloride vapor stream. Following this, they were carefully cleansed using a solution of 0.1 M SDS, ethyl alcohol, and deionized water. Ultimately, the dishes underwent a comprehensive sterilization procedure, which entailed roasting them in an oven at 110 °C for 10 hours and subjecting them to UV light for 30 minutes within a laminar flow clean bench.

## 3.2 | Growth of SH-SY5Y cells in polycarbonate culture dish

In this investigation, a freshly prepared cell suspension, characterized by a known cell concentration per milliliter using

Bio-Rad's TC20 automated cell counter, was uniformly distributed across all chambers of the culture dish. The volume of the cell suspension was carefully adjusted to maintain a consistent liquid height of approximately 2 mm in each chamber, ensuring a uniform cell surface density measured in cells per square centimeter.

Subsequently, the prepared culture dishes were positioned in a cell culture incubator set at 37 °C with a 5% $CO_2$ concentration. Systematic observation of the culture's growth transpired in all polycarbonate chambers, as well as in other mentioned bottles and dishes, employing a phase-contrast microscope. For every culture plate, five microscope images were captured — one at the plate's center and four at random locations. Post image capture, the culture plate was reinstated in the incubator, facilitating continuous and prolonged monitoring of cell growth. Microscopic image analysis enabled the determination of the average surface coverage of the culture plate over time. This analytical approach remained consistent across the majority of experiments unless explicitly indicated otherwise.

Throughout the growth process, typically extending up to 7 days, the culture medium remained unchanged unless specific alterations were mandated for a particular experiment.

## 3.3 | Measurement of the oxygen consumption rate (OCR)

To elucidate the oxygen consumption rate (OCR) in SH-SY5Y cells, we employed a Clark-type oxygen electrode, adhering to the mitochondrial function assessment protocol delineated in a previously published methodology[33]. SH-SY5Y cells were cultured in NUNC Easy Flasks (75 $cm^2$), each containing 12 ml of culture medium, until reaching approximately 90% confluence (equivalent to approximately 10 million cells per flask). Subsequently, a suspension of SH-SY5Y cells in culture medium, with concentrations of 1 million/ml and 2.5 million/ml, was introduced into the measuring chambers of the Oxygraph-2K system (Oroboros Instruments, Austria).

The determination of the non-phosphorylating leak involved the use of 4 mg/ml oligomycin, an inhibitor of mitochondrial ATP-synthase, reflecting the maximal coupled state of the mitochondria. To achieve the maximal uncoupling of the electron transfer system (ETS), we employed 1 mM FCCP (carbonyl cyanide 4-(trifluoromethoxy)phenylhydrazone). Subsequently, the residual oxygen consumption was determined by adding 2.5 mM rotenone and 0.5 mM antimycin A, inhibitors of complex I and III of the ETS, respectively.

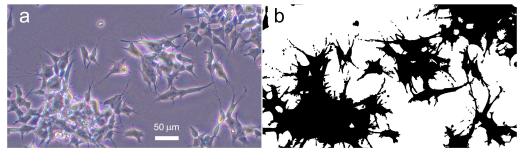


**FIGURE 2** Phase-contrast microscope image of SH-SY5Y cells (a) together with corresponding binarized picture (b).

The anticipated oxygen consumption time was estimated by utilizing the initial oxygen concentration values and the baseline OCR of the cells.

## 3.4 | Metodology of data collection

In order to delineate the developmental trajectory of cells within chambers of varying dimensions, cell images acquired on different culture days underwent binarization. This process was carried out through either manual techniques utilizing GNU Image Manipulation Program (GIMP) software or semi-automated procedures employing the phase contrast microscopy segmentation toolbox, Phantast, in ImageJ. Subsequently, Phantast-binarized images underwent manual refinements using the GIMP as necessary.

The quantification of cell-covered areas was conducted using ImageJ. The resulting values from each set of images were subjected to averaging, resulting in mean confluence measurements at distinct stages of the cell culture. An illustrative depiction of SH-SY5Y cells under phase contrast microscopy is presented in Figure 2a, while the corresponding binarized representation is showcased in Figure 2b.

## 3.5 | Monitoring SH-SY5Y Cell Growth in a Hermetically Sealed Polycarbonate Microfluidic Chip Over a One-Week Period

This investigation employs advanced biological microscopy techniques to offer real-time insights into the dynamic transformations and growth trajectories of SH-SY5Y cells within

a carefully controlled microenvironment. Captured at five-minute intervals, the resulting images were processed and condensed into a comprehensive video using ImageJ, as detailed in the Zenodo repository[31]. The hermetically sealed chip design ensures a precisely regulated environment, sustaining a consistent temperature throughout microscopic observation and obviating the necessity for chip relocation. This design decision facilitates close monitoring and exhaustive documentation of cell behavior, interactions, and growth patterns over a predetermined two-week span.

The utilized chip, integral to the research, comprises two intricately interconnected polycarbonate components securely fastened with screws and sealed with O-rings - depicted in Figure 1c, d. Prior to assembly, all elements underwent a thorough cleansing process and were annealed at 110 °C for 10 hours. Following comprehensive sterilization under UV light for 30 minutes within a laminar clean bench, the individual components were assembled. Subsequently, a 0.3 ml chamber (12 mm diameter) was filled with a cell suspension containing 1 x $10^5$ cells/ml. Prior to microscopic observarion the culture was preincubated at 37 °C, 5% $CO_2$ for 24h. The chamber was securely positioned within the microscope cabin, maintaining a constant temperature of 37 °C without $CO_2$ control. At this juncture, real-time monitoring of SH-SY5Y cell growth commenced.

## 4 | RESULTS AND DISCUSSION

### 4.1 | Exploring Seeding Concentration Effects on SH-SY5Y Cell Growth Dynamics

The investigation into the impact of seeding concentration on cell growth, particularly focusing on SH-SY5Y cells cultured in 60 mm Petri dishes at three different concentrations ($1 \times 10^4$, $5 \times 10^4$, and $1 \times 10^5$ cells/ml), provides valuable insights into the kinetics of cell proliferation. This study utilized four separate culture plates for each concentration to ensure robustness and reliability in the results. The obtained data, illustrated in Figure 3a, reveals a clear correlation between seeding concentration and the rate of cell proliferation. The microscopic images were carefully examined to assess the average surface coverage of the culture plates over time. The exponential growth kinetics displayed by SH-SY5Y cells are

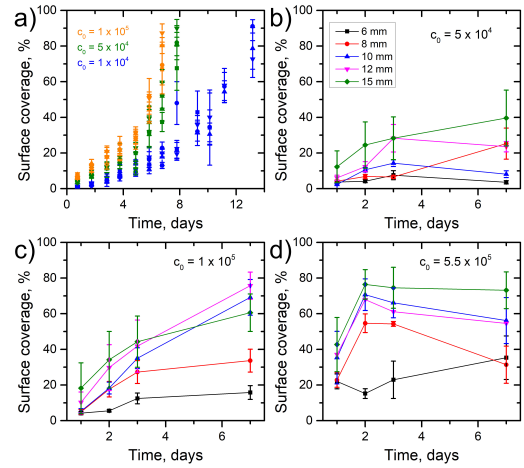


**FIGURE 3** a) The growth curve depicts the proliferation of SH-SY5Y cells on a 60 mm culture plate, initially seeded at three distinct concentrations. b) - d): Patterns of cell growth in SH-SY5Y cells (at passage 17) under varied seeding concentrations. The color-coded labeling of chamber diameters in panel b), as denoted, is consistent across panels c) and d).

particularly noteworthy.

A significant finding from this investigation is the direct relationship between seeding concentration and the speed at which full confluence is achieved. At the highest seeding concentration of $1 \times 10^5$ cells/ml, the cells reach full confluence within a relatively short timeframe of 7 days. On the other hand, the lower seeding concentration of $1 \times 10^4$ cells/ml requires a longer duration of approximately 2 weeks to attain full confluence.

This observation aligns harmoniously with the prevailing literature regarding cell culture and proliferation dynamics. According to an exhaustive study[34;35], heightened seeding concentrations have consistently shown a direct correlation with an accelerated cell growth rate and a reduced time to confluence across diverse cell lines. The study underscores the critical importance of precisely adjusting seeding density to achieve better outcomes in cell culture.

Furthermore, the investigations conducted by Johnson et al.[36] and Nirmalanandhan et al.[37] posit that increased seeding concentrations hold the potential to amplify cell proliferation rates. This phenomenon is potentially attributed to heightened cell-cell interactions and increased resource availability. Their

findings robustly reinforce the notion that elevated seeding concentrations can indeed enhance cell proliferation rates.

In conclusion, the study seems to offer meaningful insights into the impact of seeding concentration on the growth patterns of SH-SY5Y cells. The findings suggest a clear link between the initial number of cells and their proliferation rate, which appears to be in harmony with existing research on the topic. This knowledge is likely important for improving cell culture practices and for establishing more effective and consistent conditions for cell growth in future experiments.

## 4.2 | Investigating the Impact of Available Surface Area on the Growth of SH-SY5Y Cells

In our pursuit to uncover the influence of available surface area on the growth dynamics of SH-SY5Y cells, we innovatively designed and crafted polycarbonate multi-chamber culture dishes. These dishes were tailored to feature varied surfaces conducive to cell proliferation, spanning from 0.07 $cm^2$ (in circular chambers with a 3 mm diameter) to 19.63 $cm^2$ (in circular chambers with a 50 mm diameter), see Figure 1a. The through preparation of these chambers, as detailed in subsection 3.1, ensured the experimental integrity.

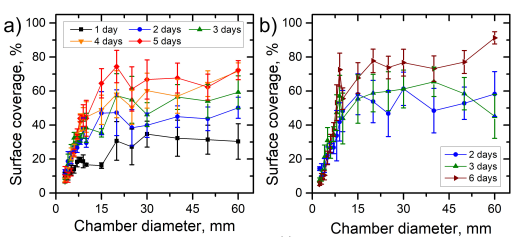


**FIGURE 4** Variations in surface coverage within cell chambers were observed in relation to chamber diameter for SH-SY5Y cells. The specific conditions, denoted by passage number and initial cell concentration, were as follows: a) SH-SY5Y p10, with an initial concentration of $1\times10^5$ cells/ml; b) SH-SY5Y p15, with an initial concentration of $5\times10^4$ cells/ml; Guide lines have been included to aid visual interpretation.

The precise calculation of cell suspension volume was executed to achieve a consistent cell suspension height of 2 mm in each chamber, thereby establishing an equivalent average surface density of cells ($1\times10^4$ cells/$cm^2$ for concentration $5\times10^4$ cells/ml) - see Table **??**. Following the seeding process, the dish was securely covered with a polycarbonate lid and incubated within a controlled cell incubator environment (37 °C / 5% $CO_2$). The progression of cell growth in each chamber was systematically observed through periodic assessments utilizing a phase-contrast microscope, conducted every 1-2 days. Graphical analysis of these microscopically captured images revealed dynamic alterations in mean cell confluence over time. Intriguingly, our findings disclosed a discernible correlation between the growth curve of SH-SY5Y cells and the available surface area for cell growth, as depicted in Figure 4.

As illustrated in Figure 4, the growth dynamics of SH-SY5Y cells within polycarbonate chambers are intricately linked to chamber dimensions. Notably, in smaller chambers with a diameter below approximately 10 - 15 mm, surface coverage exhibits a proportional scaling with chamber size. Conversely, in chambers exceeding 10 - 15 mm in diameter, surface coverage appears to be independent of chamber size, contingent solely upon the stage of culture growth. Notably, the average confluence remains consistently stable across all chambers with a diameter greater than 10 - 15 mm.

## 4.3 | Examining the Impact of Seeding Concentration on SH-SY5Y Cell Growth

In our study examining how the initial number of cells affects their growth in limited spaces, we closely monitored the growth of SH-SY5Y cells within chambers of varying diameters (6, 8, 10, 12, and 15 mm) presented in Figure 1b using distinct seeding concentrations ($5\times10^4$, $1\times10^5$, and $5.5\times10^5$ cells/ml). The consistent maintenance of a 2 mm medium height was upheld throughout the study, and microscopic images capturing the evolving cell growth were acquired at intervals of 1, 2, 3, and 7 days.

Analysis of the microscopy images, as exemplified in Figure 3 b) - d), revealed several noteworthy observations. Firstly, in chambers with a smaller diameter, such as 6 mm, cell aggregation seemed independent of seeding concentration. Despite an initial attachment of a substantial number of cells to the surface and their healthy appearance during the early stages of growth (observed at 1 and 2 days), after 3 days, only aggregated cells were discernible. Secondly, in chambers of

intermediate sizes (8 mm and 10 mm in diameter), a higher seeding concentration led to rapid cell growth, succeeded by subsequent aggregation, likely attributed to nutrient depletion in the medium. Moreover, even in chambers of intermediate size with low seeding concentration, cell aggregation could still occur. Finally, for chambers exceeding 10 mm in diameter, a seeding concentration of $1 \times 10^5$ cells/ml proved optimal for sustaining long-term observation of cell growth.

## 4.4 | The growth of HeLaGFP and 16HBE14$\sigma$ cells in polycarbonate multichamber

The growth of SH-SY5Y cells and their limited ability to adhere to surfaces, compared to other cell types, have been extensively studied by other researchers. Numerous factors, including substrate stiffness, integrin-mediated signaling, growth factors, and cell-cell interactions, have been identified as crucial in regulating the adhesive properties of SH-SY5Y cells[38;39].

Motivated by these findings, we sought to compare the growth patterns of the more adherent 16HBE14$\sigma$ and HeLaGFP cells within polycarbonate chambers subjected to experimentation (Figure 1a). The cell seeding process involved introducing cells from suspension at a concentration of $1 \times 10^5$ cells/ml. Our study involved daily, precise microscopic examinations to observe how cells were growing. The resulting growth curves, elucidated in Figure 5, offer a comprehensive depiction of the temporal evolution of cell proliferation within this experimental framework.

Our study showed that the growth of HeLaGFP cells, similar to SH-SY5Y cells, is influenced by chamber size, with a decreasing effect observed for chambers larger than 10 mm in diameter. In contrast, 16HBE14$\sigma$ cells did not show a clear growth dependence on chamber diameter. In particular, smaller chambers (diameter < 6 mm) resulted in reduced coverage after 4 days compared to 3 days for both cell lines. Nevertheless, both cell lines exhibited rapid growth, reaching 90% confluence after 4 days. Interestingly, 16HBE14$\sigma$ cells showed faster growth in polycarbonate chambers compared to HeLaGFP cells.

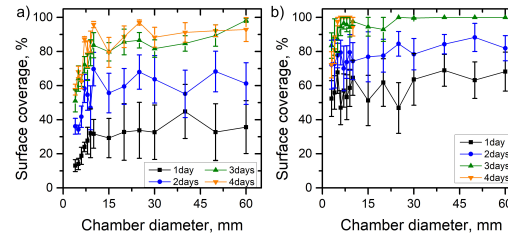


**FIGURE 5** Temporal evolution of cell growth: tracking the expansion of HeLaGFP (a) and 16HBE14$\sigma$ (b) cell populations over time, depicted as surface coverage relative to chamber diameter. The cells were initially seeded at concentration $1 \times 10^5$ cells/ml.

## 4.5 | The SH-SY5Y cells show low mitochondrial function expressed as OCR

The mitochondrial functionality within SH-SY5Y cells is distinguished by a low oxygen consumption rate (OCR), as delineated in Figure 6. The reduced respiratory activity in SH-SY5Y cells is likely due to their unique neuronal characteristics, increased sensitivity to oxidative stress, and possible mitochondrial issues. This is shown by lower levels of ATP, mitochondrial membrane potential (MMP), and citrate synthase activity[40;41].

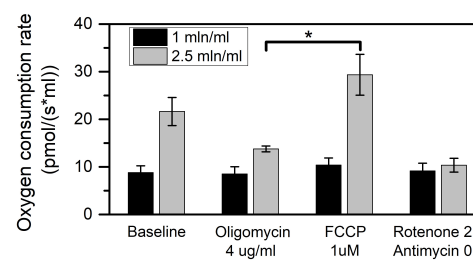


**FIGURE 6** Oxygen consumption rate in SH-SY5Y cells: The depicted bars illustrate the OCR for two cell concentrations — $1 \times 10^6$ cells/ml (black bars) and $2.5 \times 10^6$ cells/ml (grey bars). Results are presented as means ± standard error of the mean (SEM), with a sample size of $n = 4$ for the former and $n = 3$ for the latter. Statistical significance, denoted by (*), was determined at $p < 0.05$ using one-way analysis of variance (ANOVA).

We investigated the oxygen consumption dynamics of SH-SY5Y cells during cellular respiration. The baseline oxy-

gen consumption rate (OCR) for 1 million cells/ml was 8.8 pmol/(s*ml). Oligomycin, an ATP synthase inhibitor, reduced the OCR to 8.5 pmol/(s*ml) by blocking proton flow to the mitochondrial matrix. FCCP, an uncoupler, increased OCR to 10.4 pmol/(s*ml). There was no significant difference between the effects of FCCP and baseline OCR or OCR after oligomycin. Interestingly, a 2.5-fold higher cell concentration resulted in more than a 2-fold increase in OCR after FCCP compared to oligomycin. Baseline OCR also increased 2.5-fold at higher cell concentrations, indicating a linear correlation between OCR and cell concentration. In the final phase, rotenone and antimycin A inhibited complexes I and III in the ETS, respectively, impeding electron flow and facilitating measurement of extra-mitochondrial oxygen consumption.

**TABLE 1** Anticipated duration of oxygen utilization by SH-SY5Y cells at varied abundances in the culture medium, assuming no air exchange. The presented table displays results averaged to two significant digits.

| | $10^4$ cells/ml | $10^6$ cells/ml |
|---|---|---|
| $O_2$ conc. (pmol/ml) | 220000 | 220000 |
| OCR (pmol/s*ml) | 0.088 | 8.8 |
| OCT (s) | 2500000 | 25000 |
| OCT (min.) | 42000 | 420 |
| OCT (h) | 700 | 7 |
| OCT (days) | 29 | 0.29 |

$O_2$ conc., initial oxygen concentration in the culture medium; OCR, oxygen consumption rate; OCT, oxygen consumption time.

The expected duration of oxygen consumption for different concentrations of SH-SY5Y cells is shown in Table 1. Specifically, the approximate time for oxygen consumption is 29 days for a cell concentration of $10^4$ cells/ml and 2.9 days for a concentration of $10^6$ cells/ml. These results are consistent with the baseline Oxygen Consumption Rate (OCR) exhibited by the cells as shown in Figure 6. It is important to note that the estimated oxygen consumption time was derived from a linear relationship and did not control for cell division. To improve the accuracy of our understanding of oxygen consumption, it is important to include the rate of cell division when calculating the corrected OCR. In addition, the diffusion of oxygen within the polycarbonate system should be carefully considered to ensure a more accurate representation of the overall oxygen dynamics in the experimental setup.

## 4.6 | Long, real time microscopic observation of the growth of SH-SY5Y cells in sealed chamber

In the initial phase of cultivating SH-SY5Y cells on microfluidic chips, the authors conducted preliminary tests using small chambers with a 0.5 mm diameter. Unfortunately, no observable cell growth was evident in these chambers. Subsequent investigations demonstrated a notable preference of SH-SY5Y cells for chambers with diameters exceeding 10 mm. Building upon these insights, a carefully designed, sealed chamber with a 12 mm diameter and a volume of 0.3 ml was crafted - compare Figure 1c, d. Continuous microscopic monitoring of SH-SY5Y cell growth dynamics within this chamber was then undertaken.

This study aimed to precisely track the real-time microscopic development of cells without external gas exchange. The chamber volume of 0.3 ml was chosen based on cellular respiration results and the requirement for observations spanning at least one week. Consequently, the chip's chamber exhibits a cell surface density of 200 cells/mm$^2$ at the outset.

Figure 7a shows how the surface coverage in the chip chamber changes over time. Comparing a sealed 12 mm diameter chamber with a standard culture chamber, the area covered by cells was similar on days 2, 3 and 7 of the culture period, as shown in Figure 3c. This suggests that the long-term culture of cells with air exchange through the medium is comparable to the conventional method of culture in sealed chambers.

In addition, the morphological behaviour of SH-SY5Y cells during long-term culture was investigated (see Figure 7b). The morphological transformation of a dividing cell from a stretched surface configuration to a spherical shape was observed. The process of cell division is illustrated in Figure 7b20-b45, showing the positioning of chromosomes and the inclusion of temporal markers to indicate the dynamics of the process. After division, the spherical cells return to their stretched form on the surface. To our knowledge, this morphological feature of SH-SY5Y cell division has not yet been reported.

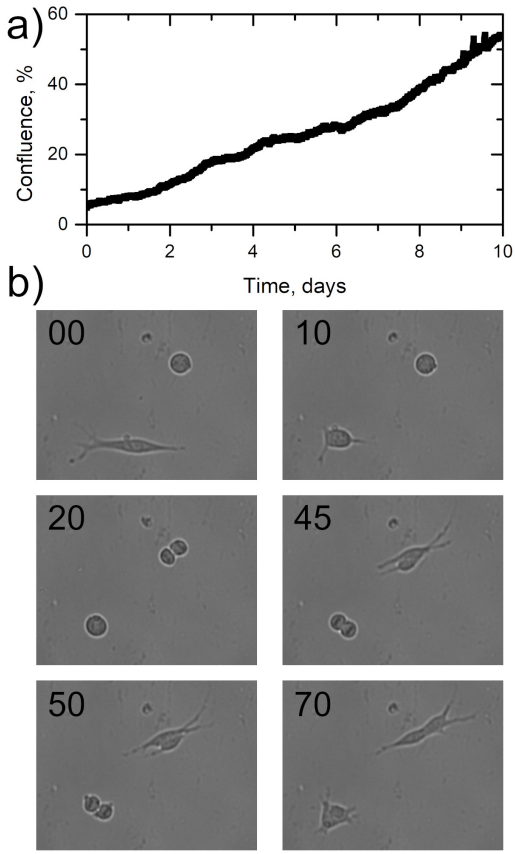


**FIGURE 7** a) The graph illustrates the temporal evolution of surface coverage within the on-chip chamber. b) The cultivation of SH-SY5Y cells is depicted, revealing discernible morphological transformations—from an elongated surface configuration to a spherical shape—and the distinctive positioning of chromosomal lines within the cell both pre and post-division. Each individual image is temporally annotated in minutes, relative to the initial photograph.These individual frames are extracted from a video available in the Zenodo repository.[31]

## 5 | CONCLUSIONS

Herein, we examined how SH-SY5Y neuroblastoma cells grow in custom-designed chambers. Our initial findings showed that these cells proliferate more slowly in small chambers. As a result, we embarked on a precise calibration process to identify the ideal chamber size.

The study investigated how the initial concentration of seeds affects the growth rate of cells. It found a clear connection between higher concentrations and faster cell proliferation, which aligns with existing research.

Additionally, the impact of available surface area on SHSY5Y cell growth was investigated revealing that the use of polycarbonate chambers approximately 10 mm in diameter results in a cell proliferation rate similar to that seen in standard 60 mm Petri dishes. This finding has important implications for improving cell culture techniques, as it suggests that smaller chambers create unfavorable conditions for cell proliferation. While the main focus was on SH-SY5Y, similar patterns were observed for HeLaGFP. In contrast, 16HBE14$\sigma$ cells showed no dependence on proliferation changes based on chamber diameter.

The study revealed that SH-SY5Y cells have low mitochondrial function, as evidenced by their reduced oxygen consumption rate. This unique respiratory property makes them ideal for long-term studies in sealed chambers. Observations support the practicality of culturing these cells in large sealed plastic chambers (minimum diameter: 10 mm). The choice of rigid polymers over softer polymers such as PDMS with higher gas permeability streamlines experimental setups and increases the practicality of the microfluidic platform[42].

In addition, a morphological change in SH-SY5Y cell shape, from stretched to spherical, was observed during cell division. After division, the cells reverted to their original shape.

These findings seem important for researchers in fields such as neuroscience, cell biology, and bioengineering. They provide clear guidelines for improved experimental design and execution. The demonstrated adaptability of SH-SY5Y cells to different culture conditions opens up possibilities for novel research methods, contributing to the advancement of cellular research.

## AUTHOR CONTRIBUTIONS

EK: conceptualization, formal analysis, data curation, investigation, methodology, writing – original draft, and writing – review & editing; AL: formal analysis, data curation, investigation, methodology; DW: formal analysis, data curation, investigation, methodology; WS: formal analysis, data curation; JA: formal analysis, data curation; PZ: conceptualization,

writing – original draft, and writing – review & editing; SJ: conceptualization, funding acquisition, investigation, methodology, project administration, resources, supervision, writing – original draft, and writing – review & editing.

## CONFLICTS OF INTEREST

There are no conflicts to declare.

## DATA AVAILABILITY STATEMENT

Two Zenodo repositories [30;31] contain the original files used to prepare the figures and formulate the conclusions.

## REFERENCES


1. Lee J, Cuddihy MJ, and Kotov NA. Three-Dimensional Cell Culture Matrices: State of the Art. Tissue Engineering Part B: Reviews. 2008 Mar;**14**(1):61–86. Publisher: Mary Ann Liebert, Inc., publishers.

2. Damiati S, Kompella UB, Damiati SA, and Kodzius R. Microfluidic devices for drug delivery systems and drug screening. Genes. 2018;**9**(2):103.

3. Arandian A, Bagheri Z, Ehtesabi H, Najafi Nobar S, Aminoroaya N, Samimi A, et al. Optical Imaging Approaches to Monitor Static and Dynamic Cell-on-Chip Platforms: A Tutorial Review. Small. 2019;**15**(28):1900737.

4. Yonet-Tanyeri N, Amer M, Balmert SC, Korkmaz E, Falo LDJ, and Little SR. Microfluidic Systems For Manufacturing of Microparticle-Based Drug-Delivery Systems: Design, Construction, and Operation. ACS Biomaterials Science & Engineering. 2022 Jul;**8**(7):2864–2877.

5. Leung CM, de Haan P, Ronaldson-Bouchard K, Kim GA, Ko J, Rho HS, et al. A guide to the organ-on-a-chip. Nature Reviews Methods Primers. 2022 May;**2**(1):1–29.

6. Amirifar L, Shamloo A, Nasiri R, de Barros NR, Wang ZZ, Unluturk BD, et al. Brain-on-a-chip: Recent advances in design and techniques for microfluidic models of the brain in health and disease. Biomaterials. 2022 Jun;**285**:121531.

7. Dugger BN, and Dickson DW. Pathology of neurodegenerative diseases. Cold Spring Harbor perspectives in biology. 2017;**9**(7):a028035.

8. Wilson DM, Cookson MR, Van Den Bosch L, Zetterberg H, Holtzman DM, and Dewachter I. Hallmarks of neurodegenerative diseases. Cell. 2023;**186**(4):693–714.

9. Slanzi A, Iannoto G, Rossi B, Zenaro E, and Constantin G. In vitro models of neurodegenerative diseases. Frontiers in cell and developmental biology. 2020;**8**:328.

10. Gangras P, Gelfanova V, Williams GD, Handelman SK, Smith RM, and Debets MF. Investigating SH-SY5Y Neuroblastoma Cell Surfaceome as a Model for Neuronal-Targeted Novel Therapeutic Modalities. International Journal of Molecular Sciences. 2022 Jan;**23**(23):15062.

11. Lopes FM, Schröder R, da Frota Júnior MLC, Zanotto-Filho A, Müller CB, Pires AS, et al. Comparison between proliferative and neuron-like SH-SY5Y cells as an in vitro model for Parkinson disease studies. Brain research. 2010;**1337**:85–94.

12. Xicoy H, Wieringa B, and Martens GJ. The SH-SY5Y cell line in Parkinson's disease research: a systematic review. Molecular neurodegeneration. 2017;**12**:1–11.

13. Constantinescu R, Constantinescu A, Reichmann H, and Janetzky B. Neuronal differentiation and long-term culture of the human neuroblastoma line SH-SY5Y. Springer; 2007.

14. Alrashidi H, Eaton S, and Heales S. Biochemical characterization of proliferative and differentiated SH-SY5Y cell line as a model for Parkinson's disease. Neurochemistry International. 2021;**145**:105009.

15. Agholme L, Lindström T, Kågedal K, Marcusson J, and Hallbeck M. An in vitro model for neuroscience: differentiation of SH-SY5Y cells into cells with morphological and biochemical characteristics of mature neurons. Journal of Alzheimer's disease. 2010;**20**(4):1069–1082.

16. de Medeiros LM, De Bastiani MA, Rico EP, Schonhofen P, Pfaffenseller B, Wollenhaupt-Aguiar B, et al. Cholinergic differentiation of human neuroblastoma SH-SY5Y cell line and its potential use as an in vitro model for Alzheimer's disease studies. Molecular Neurobiology. 2019;**56**:7355–7367.

17. Jucker M, and Walker LC. Self-propagation of pathogenic protein aggregates in neurodegenerative diseases. Nature. 2013;**501**(7465):45–51.

18. Vaquer-Alicea J, and Diamond MI. Propagation of protein aggregation in neurodegenerative diseases. Annual review of biochemistry. 2019;**88**:785–810.

19. Pantiya P, Thonusin C, Chattipakorn N, and Chattipakorn SC. Mitochondrial abnormalities in neurodegenerative models and possible interventions: Focus on Alzheimer's disease, Parkinson's disease, Huntington's disease. Mitochondrion. 2020;**55**:14–47.

20. Grel H, Woznica D, Ratajczak K, Kalwarczyk E, Anchimowicz J, Switlik W, et al. Mitochondrial Dynamics in Neurodegenerative Diseases: Unraveling the Role of Fusion and Fission Processes. International Journal of Molecular Sciences. 2023;**24**(17):13033.

21. Li R, Zhang X, Lv X, Geng L, Li Y, Qin K, et al. Microvalve controlled multi-functional microfluidic chip for divisional cell co-culture. Analytical biochemistry. 2017;**539**:48–53.

22. Lesniak A, Kilinc D, Blasiak A, Galea G, Simpson JC, and Lee GU. Rapid Growth Cone Uptake and Dynein-Mediated Axonal Retrograde Transport of Negatively Charged Nanoparticles in Neurons Is Dependent on Size and Cell Type. Small. 2019;**15**(2):1803758.

23. Kim S, Kang S, Choe J, Moon C, Choi H, Kim JY, et al. A Microfluidic System for Investigating Anticipatory Medication Effects on Dopamine Homeostasis in Dopaminergic Cells. Analytical Chemistry. 2023;**95**(6):3153–3159.

24. Yeste J, García-Ramírez M, Illa X, Guimerà A, Hernández C, Simó R, et al. A compartmentalized microfluidic chip with crisscross microgrooves and electrophysiological electrodes for modeling the blood–retinal barrier. Lab on a Chip. 2018;**18**(1):95–105.

25. Wen X, Takahashi S, Hatakeyama K, and Kamei Ki. Evaluation of the effects of solvents used in the fabrication of microfluidic devices on cell cultures. Micromachines. 2021;**12**(5):550.

26. Li R, Lv X, and Deng Y. NOA 81 fabricated microfluidic chip for SH-SY5Y cell culture. In: 2015 IEEE International Conference on Mechatronics and Automation (ICMA). IEEE; 2015. p. 994–998.

27. Dinh ND, Chiang YY, Hardelauf H, Baumann J, Jackson E, Waide S, et al. Microfluidic construction of minimalistic neuronal co-cultures. Lab on a Chip. 2013;**13**(7):1402–1412.

28. Bengoa-Vergniory N, Faggiani E, Ramos-Gonzalez P, Kirkiz E, Connor-Robson N, Brown LV, et al. CLR01 protects dopaminergic neurons in vitro and in mouse models of Parkinson's disease. Nature communications. 2020;**11**(1):4885.

29. Bastiaens A, Sabahi-Kaviani R, and Luttge R. Nanogrooves for 2D and 3D microenvironments of SH-SY5Y cultures in brain-on-chip technology. Frontiers in Neuroscience. 2020;**14**:666.

30. Kalwarczyk E, and Jakiela S. Exploring Cellular Dynamics: A Comprehensive Analysis of SH-SY5Y Cell Growth in Variable Polycarbonate Chambers and Comparative Insights with Standard Petri Dishes. Zenodo. 2023;p. https://zenodo.org/records/10401181.

31. Woznica D, and Jakiela S. SH-SY5Y cell proliferation within a hermetically sealed polycarbonate chamber for a duration of two weeks. Zenodo. 2023;p. https://zenodo.org/records/10418022.

32. Singh A, Maity A, and Singh N. Structure and Dynamics of dsDNA in Cell-like Environments. Entropy. 2022 Nov;**24**(11):1587.

33. Brand MD, and Nicholls DG. Assessing mitochondrial dysfunction in cells. Biochemical Journal. 2011;**435**(2):297–312.

34. Stiehler M, Bünger C, Baatrup A, Lind M, Kassem M, and Mygind T. Effect of dynamic 3-d culture on proliferation, distribution, and osteogenic differentiation of human mesenchymal stem cells. Journal of Biomedical Materials Research Part A. 2008;**89A**:96–107.

35. Vlodavsky I, Voss R, Yarkoni S, and Fuks Z. Stimulation of human amniotic fluid cell proliferation and colony formation by cell plating on a naturally produced extracellular matrix. Prenatal Diagnosis. 1982;**2**:13–23.

36. Johnson KE, Howard G, Mo W, Strasser MK, Lima EABF, Huang S, et al. Cancer cell population growth kinetics at low densities deviate from the exponential growth model and suggest an Allee effect. PLOS Biology. 2019 Aug;**17**(8):e3000399. Publisher: Public Library of Science.

37. Nirmalanandhan VS, Levy MS, Huth AJ, and Butler DL. Effects of cell seeding density and collagen concentration on contraction kinetics of mesenchymal stem cell–seeded collagen constructs. Tissue Engineering. 2006;**12**:1865–1872.

38. Li Y, Xiong H, and Yang DQ. Functional switching of ATM: sensor of DNA damage in proliferating cells and mediator of Akt survival signal in post-mitotic human neuron-like cells. Chinese Journal of Cancer. 2012 Aug;**31**(8):364–372.

39. Dwane S, Durack E, and Kiely PA. Optimising parameters for the differentiation of SH-SY5Y cells to study cell adhesion and cell migration. BMC Research Notes. 2013 Sep;**6**(1):366.

40. Dieter F, Esselun C, and Eckert GP. Redox Active $\alpha$-Lipoic Acid Differentially Improves Mitochondrial Dysfunction in a Cellular Model of Alzheimer and Its Control Cells. International Journal of Molecular Sciences. 2022 Jan;**23**(16):9186.

41. Li YJ, Zhan Y, Li C, Sun J, and Yang C. CPI-1189 protects neuronal cells from oxygen glucose deprivation/reoxygenation-induced oxidative injury and cell death. Aging. 2021 Feb;**13**(5):6712–6723.

42. Rein C, Toner M, and Sevenler D. Rapid prototyping for high-pressure microfluidics. Scientific Reports. 2023 Jan;**13**(1):1232.